ADVANCED ELECTRONIC MATERIALS
www.advelectronicmat.de

Transient Extraction of Holes and Electrons Separately Unveils the Transport Dynamics in Organic Photovoltaics

Jiajun Peng, Xiaoqing Chen, Yani Chen, Oskar J. Sandberg, Ronald Österbacka, and Ziqi Liang**

We have utilized the metal–insulator–semiconductor charge extraction by linearly increasing voltage (MIS-CELIV) technique to clarify the hole- and electron-transport properties in benchmark poly(3-hexylthiophene) (P3HT) and its blend with phenyl-C61-butyric acid methyl ester (PCBM) by using a thick lithium fluoride (LiF) as the charge-blocking layer. Both dark and light MIS-CELIV are employed to comparatively investigate the differences in the recombination process and charge mobilities in neat P3HT and P3HT:PCBM blends. Our studies quantitatively show that balanced hole and electron transport can be achieved in the P3HT:PCBM blend under light illumination, leading to a high efficiency in the photovoltaic cell. Furthermore, light MIS-CELIV can be employed as a novel method to directly evaluate the capability of photoelectric conversion of organic photovoltaic materials.

1. Introduction

In recent years, a steady increase has been reported in the power-conversion efficiency (PCE) of solution-processed organic photovoltaic (OPV) cells with double-layer or bulk heterojunction (BHJ) architectures.[1–3] The PCE of OPV cells is mainly determined by three factors: the open-circuit voltage (V_{oc}), short-circuit current density (J_{sc}), and fill factor (FF).[4–6] By choosing designed photovoltaic materials with varying electronic band structures, the V_{oc}, which is determined by the energy level difference between the donor and acceptor materials, and J_{sc}, which is characteristic of light absorption, can both be greatly increased to enhance the cell performance.[7–10] By contrast, the FF generally reflects the dynamics of the charge transport and recombination.[11] For instance, the large contact barriers and imbalance between the electron and hole mobilities, which are often found in OPV cells, largely reduce the FF.[12] It is thus necessary to probe and reveal the dynamics of the charge-transport process in OPVs.[13–17]

J. Peng, Dr. X. Chen, Y. Chen, Prof. Z. Liang
Department of Materials Science
Fudan University
Shanghai 200433, P. R. China
E-mail: zqliang@fudan.edu.cn
Mr. O. J. Sandberg, Mr. R. Österbacka
Center for Functional Materials and Department of Natural Sciences
Åbo Akademi University
Turku 20500, Finland
E-mail: ronald.osterbacka@abo.fi

DOI: 10.1002/aelm.201500333

There are various methods of studying the transport dynamics while measuring the charge-carrier mobility in organic semiconductors,[18,19] including space-charge limited current (SCLC),[20–22] charge extraction by linearly increasing voltage (CELIV),[23–26] time-of-flight (TOF),[27–29] and field-effect transistor (FET) studies.[30,31] Each of these four methods has its own merits and limitations for its applied range. 1) The most widely used method is SCLC, which can measure the hole and electron mobility in hole-only and electron-only devices, respectively. Because a charge injection contact is critical in SCLC measurements, the SCLC technique cannot be used to measure the hole mobility in organic semiconductors with a deep highest occupied molecular orbital (HOMO) energy level, nor measure the electron mobility with a high lowest unoccupied molecular orbital (LUMO) energy level.[20–22] More reliable methods of studying the charge transport in OPVs are CELIV and TOF, which are compatible with most p-conjugated polymers.[14,32] 2) CELIV can determine the charge mobility in the original device structure of a working solar cell; moreover, the thickness of the active layer is flexible in the range of 100 nm to 1 μm. CELIV measurement mainly includes three methods: a) dark-CELIV with intrinsic impurities-induced charge carriers, b) photo-CELIV[33,34] with photo-generated charge carriers, and c) i-CELIV (injection-CELIV)[35,36] with electrically-injected charge carriers by applied voltage offsets. Note that dark-CELIV only measures the mobility of equilibrium charge carriers, whereas photo-CELIV only measures the mobility of photo-generated charge carriers.[18] However, all these CELIV measurements cannot distinguish between the type of present hole or electron carriers. 3) By contrast, TOF can selectively measure the hole or electron mobility.[37,38] However, a thick film on the order of several micrometers is often required in order to allow for the photogenerated charge carriers to reach quasi-equilibrium and obtain accurate values of the charge mobility. 4) The FET method, on the other hand, is widely used to simultaneously measure in-plane hole and electron mobilities of organic semiconductors.

Recently, a novel technique based on CELIV yet in a metal–insulator–semiconductor (MIS) diode structure (namely MIS-CELIV), was invented by Juška and Sandén independently and later applied by Armin et al. using a blocking layer of MgF_2 to study the charge transport in organic solar cells in the dark.[39–42]

The unique advantage of MIS-CELIV is that it can measure the hole and electron mobilities independently by using different device configurations. Moreover, MIS-CELIV allows for the measurement of electrically-injected charge carriers in the dark, whereas both photo-CELIV and TOF rely upon light excitation to generate free charge carriers. In the latter techniques, owing to the presence of non-equilibrium transport in thin films, it is difficult to obtain accurate values of the charge mobility.

In our work, as opposed to Armin's work, the MIS-CELIV technique was modified by using a thick lithium fluoride (LiF) layer of around 140 nm as the blocking layer in an OPV cell to measure the hole and electron mobility both in the dark and under light illumination. An ultrathin LiF layer (ca. 1–2 nm) is known to act as a stable and transparent buffer layer for the metal cathode in normal OPV cells to improve the device performance, which has been believed to originate from electron tunneling or dipole formation.[43] The thick LiF layer introduced in our work can effectively block a certain type of charge carriers (either hole or electron). As a result, the electron or hole mobility can be measured from electron-only or hole-only MIS-diodes, respectively. Our proof-of-concept demonstrations based on benchmark poly(3-hexylthiophene) (P3HT) and its blend with phenyl-C61-butyric acid methyl ester (PCBM) (P3HT:PCBM) unravel the transport dynamics in OPVs. Furthermore, we applied MIS-CELIV under laser light illumination, in which photo-generated carriers can be clearly distinguished from electrically injected carriers by comparing the areas of the extracted current density versus time curves (namely, *j-t* profiles) between the dark and light MIS-CELIV.

2. Results and Discussion

2.1. MIS-CELIV Experiments

As illustrated in **Figure 1**, hole-only and electron-only MIS diodes were made with device configurations of ITO/active layer (120 nm)/LiF (140 nm)/Al (100 nm) (Figure 1a) and ITO/LiF (140 nm)/active layer (120 nm)/LiF (1 nm)/Al (100 nm) (Figure 1b), respectively. Note that the 140 nm-LiF interlayer plays a very important role in charge blocking in the MIS-CELIV.

The reason why MIS-CELIV can individually measure hole or electron mobilities with different structures is schematically illustrated in Figure 1. The holes drift towards the ITO (negative) electrode whereas the electrons drift towards the Al (positive) electrode under the applied electric field. The role of the thick LiF layer (ca. 140 nm thick) lies in the fact that it can effectively block electrons or holes when the charge carriers drift towards the LiF layer; consequently, certain charge carriers will not be able to traverse the neighboring Al or ITO electrode and therefore do not contribute to the measured transient currents. Hence, when LiF is placed below the Al electrode, all the electrons are blocked and only holes can be measured in the hole-only device, as shown in Figure 1a. Likewise, when a thick LiF interlayer is placed above the ITO electrode, all the holes are blocked and only electrons can be measured in the electron-only device, as shown in Figure 1b.

To help understand the working mechanism, the experimental setup of MIS-CELIV for selective hole- or electron-mobility measurements is schematically depicted in **Figure 2**. Figure 2a illustrates the triangle voltage pulse with varying voltage offsets in reverse bias, including low, moderate, and large offsets. Figure 2b shows the corresponding MIS-CELIV transients at different levels of voltage offsets. In Figure 2a, linearly increasing voltages with various bias offsets are applied to the MIS-CELIV devices, thereby electrically injecting various quantities of charge carriers to regulate the charge-carrier density in the device. The triangle voltage pulse was used to extract the internal charge carriers, both the electrically-injected and photo-generated charge carriers. As illustrated in Figure 2b, the current transient begins at the displacement level as determined by the total capacitance of the device and the slope of the applied voltage. If the transient current saturates to the value of the displacement current at the end of the voltage ramp, this indicates that the LiF layer is able to block the charge injection at higher applied voltages. It is also important to evaluate whether the current density before the voltage ramp is zero, thus ensuring the accuracy of the measured mobilities. At low voltage offsets, the current peaks at the transit time (t_{tr}), and then drops to the displacement current when the entire device becomes depleted. By applying a moderate or large voltage offset, the time at which the peak current is achieved is larger than t_{tr}, and the overall amount of extracted carriers increases due to additional electrically injected charge carriers.[39]

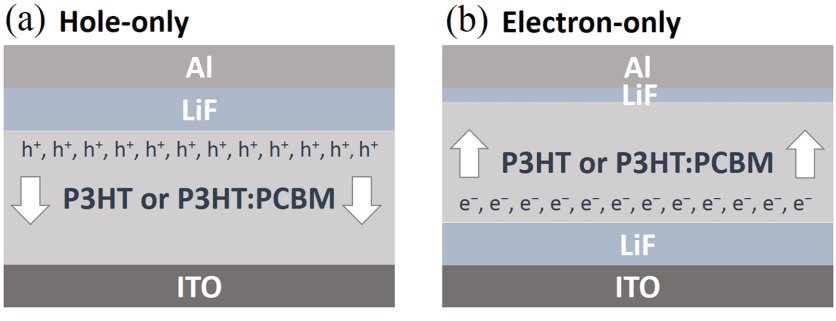

Figure 1. a,b) Schematic of MIS-CELIV for hole-only (a) and electron-only (b) configurations. The hole or electron mobility could be measured from the hole-only or electron-only MIS-diode. The electrically-injected or photo-generated charge carriers were mainly distributed near the interface of the insulator/semiconductor.

2.2. Advantages of MIS-CELIV

Conventional CELIV can only measure the average of both carrier mobilities, but the individual contribution from the holes and electrons remains unclear. If the lifetime of the charge carriers is significantly shorter than the applied delay time, the maximum current density, shown as the bump in the photo-CELIV curve, triggered by the laser light is greatly reduced due to charge recombination and hence t_{tr} is hard to verify. An alternatively better approach to measuring t_{tr} is to increase the offset voltage and thus

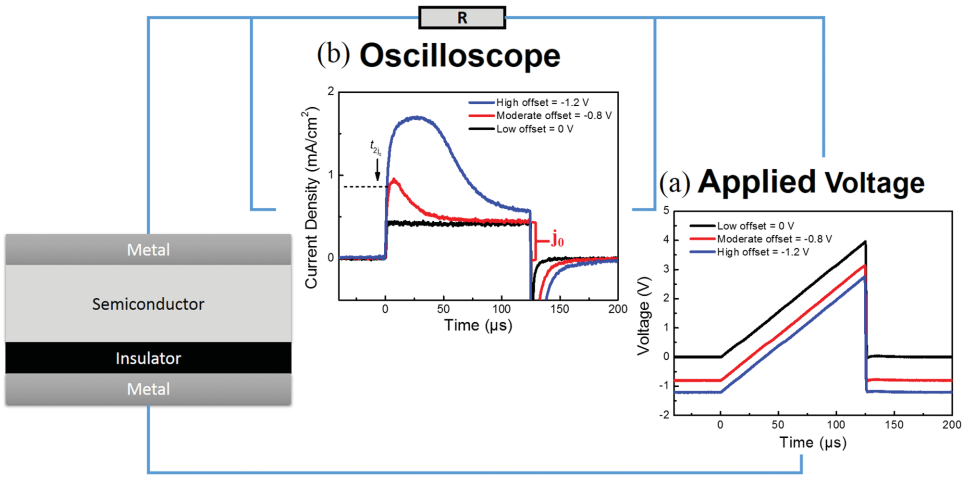

Figure 2. Experimental setup of MIS-CELIV for selective hole or electron mobility measurement. a) Applied CELIV triangle pulses with varying voltage offsets in reverse bias. b) MIS-CELIV transients at different levels of voltage offsets in reverse bias.

the current increases to the maximum current density (j_∞). Then there are enough extracted charge carriers in the semiconductor to be screened by the electric field.[39] As is shown in Figure 2b, both dark and light MIS-CELIV can be used to apply the moderate voltage offsets to readily obtain t_{tr} from t_{2j0} by the following equation under the condition of $\frac{j_\infty}{j_0} \gg 1$,[39]

$$t_{tr} = \frac{4}{\pi} \cdot t_{2\,j0} \tag{1}$$

where t_{2j0} is the time at which the current density reaches $j = 2j_0$, and j_0 is the displacement current corresponding to the capacitance of the entire diode including both the semiconductor and insulator layers.

Equation (2)[39] can be used to calculate the charge mobility from MIS-CELIV measurements if $\frac{j_\infty}{j_0} \gg 1$, when the semiconductor layer is a few times thicker than the insulator layer, or when the dielectric constant of the insulator is higher than the semiconductor.[39] In this work, the dielectric constant of the insulator layer LiF is 9,[43] whereas that of the semiconductor layer is 3.4,[14] so the conditions of Equation (2) are fulfilled and it can be written as:

$$\mu = \frac{2d_s^2}{\left(At_{tr}^2\right)\left(1+\frac{\epsilon_s d_i}{\epsilon_i d_s}\right)} \tag{2}$$

where d_s is the thickness of the semiconductor layer, d_i is the thickness of the insulator layer, ϵ_s is the dielectric constant of the semiconductor layer, ϵ_i is the dielectric constant of the insulator layer, μ is the charge carrier mobility, and A is the voltage ramp ($A = \mathrm{d}U/\mathrm{d}t$). Note that $\left(1+\frac{\epsilon_s d_i}{\epsilon_i d_s}\right)$ was calculated to be 1.44 in our measurements of both hole and electron mobilities according to the above dielectric constants and the film thickness. The j_0 could be retrieved from the initial step at $t = 0$, which remained steady in the same device structure under different voltage offsets. According to our light MIS-CELIV results, j_0 also did not change when light was applied. As a result, Equation (2) can be used for both dark and light MIS-CELIV to calculate the charge mobility.

Compared to conventional CELIV techniques, the dark and light MIS-CELIV methods allow for the selective measurement of either the electron or hole mobility by using different diode structures. Note that in light MIS-CELIV, although both holes and electrons are photogenerated in the active layer by light illumination, one type of charge carrier can be successfully blocked by the thick LiF layer at one surface in the charge-extraction process. Therefore, with only one specified type of charge carriers being injected or extracted from the sample, the interpretation of MIS-CELIV from such device configuration is simplified as there is no interference from the other charge-carrier type.

2.3. Dark and Light MIS-CELIV

A combination of dark and light MIS-CELIV is applied to reveal the influence of light illumination on charge mobility of investigated organic semiconductors. We applied dark MIS-CELIV to P3HT and a P3HT:PCBM blend devices in our studies, as shown in **Figure 3** and **Figure 4**, respectively. The dark MIS-CELIV transients of hole-only and electron-only P3HT devices at various offsets are shown in Figure 3a and b, respectively. The mobility value was calculated from the results with moderate offsets according to Equation (1) and Equation (2). The maximum current density and the corresponding time value increased significantly when the offset was increased. Moreover, for the P3HT:PCBM blend, the dark MIS-CELIV transients at various offsets in hole-only and electron-only devices are shown in Figure 4a and 4b, respectively. All the above mobility results of hole and electron in the dark MIS-CELIV are summarized in **Table 1**. Also, as seen from Figure 4a, some unintentional doping exists in the hole-only P3HT:PCBM device. The back-ground hole doping concentration is estimated to be ~6×10^{16} cm^{-3}, according to Equation (3), which is low enough to ensure the accuracy of hole mobility measurements.[18]

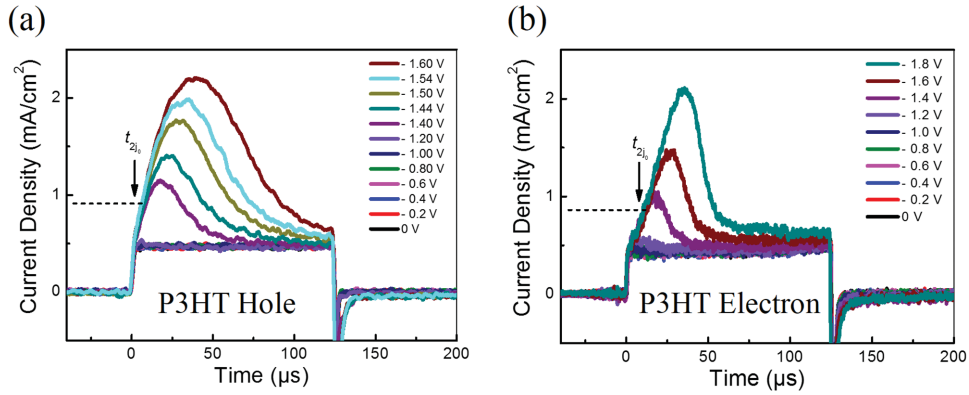

Figure 3. Dark MIS-CELIV transients of P3HT. Transients at various voltage offsets in a) hole-only and b) electron-only devices.

$$\sigma = \mu ne \tag{3}$$

where σ is the conductivity of the semiconductor, μ is the mobility of the dominant charge carriers, n is the charge-carrier density, and e is the elementary charge.

This MIS-CELIV method was further combined with pulsed laser light MIS-CELIV,[44] and found to be effective in examining the proportion of photo-generated carriers compared to the electrically injected carriers. The light MIS-CELIV method was applied to the P3HT device, as shown in **Figure 5**. The light MIS-CELIV transients of hole-only and electron-only P3HT devices with various delay times without voltage offset are shown in Figure 5a and c, respectively. The black curve represents the dark MIS-CELIV measurement results. The colored curves are the light MIS-CELIV measurement results at various delay time from 50 μs to 50 ms without voltage offset. The light MIS-CELIV transients at different voltage offsets and with the same delay time of 50 μs in hole-only and electron-only devices of P3HT are shown in Figure 5b and d, respectively.

Furthermore, light MIS-CELIV was also applied to the P3HT:PCBM blend device as shown in **Figure 6**. The dependence of the light MIS-CELIV in hole-only devices on the delay time (voltage offset = 0 V) and on the voltage offsets (delay time = 50 μs) are presented in Figure 6a and b, respectively, whereas the results of the electron-only device are presented in Figure 6c and d, respectively. The results of the hole and electron mobilities using light MIS-CELIV in both the P3HT and P3HT:PCBM devices are summarized in **Table 2**.

2.4. Implications of MIS-CELIV

It can clearly be seen that the current densities of the P3HT:PCBM blend film in both the hole-only (Figure 5a and 6a) and electron-only (Figure 5c and 6c) devices are more than doubled compared to those of the neat P3HT film. The reason for this is that the photo-generated charge transfer from P3HT to PCBM in the blend greatly enhanced the charge-separation efficiency, leading to significantly increased current densities of the free charge carriers.

As shown in Figure 6a and c, the *j-t* profiles of the P3HT:PCBM blend show a strong dependence on the delay time without voltage offset,[45] that is, the current density decreased gradually as the delay time increased. By contrast, the maximum current density decreased slightly in the case of the P3HT hole-only device, as seen from Figure 5a. These two phenomena indicate that the charge-recombination process is faster in P3HT:PCBM than in P3HT; in other words, the lifetime of the charge carriers in P3HT:PCBM is shorter.

As can be seen in Tables 1 and 2, the hole and electron mobilities of P3HT and P3HT:PCBM were both consistent with our conventional CELIV results and also in good agreement with literature results on both TOF and CELIV.[46–52] More

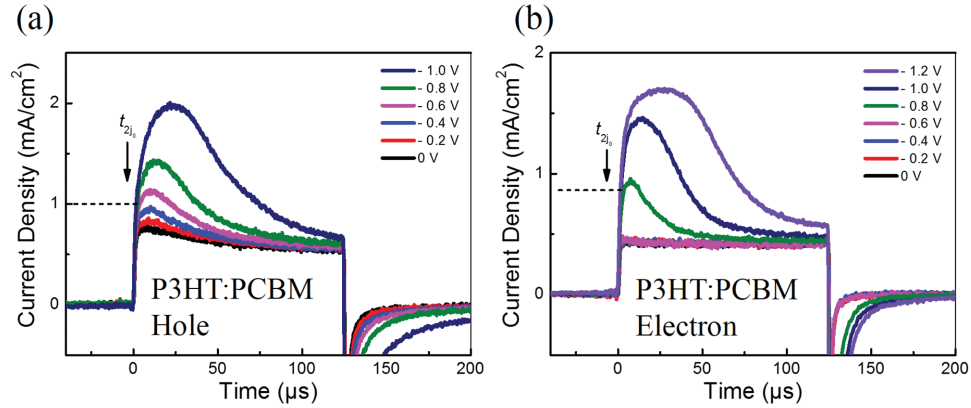

Figure 4. Dark MIS-CELIV transients of a P3HT:PCBM blend. Transients at various voltage offsets in a) hole-only and b) electron-only devices.

Table 1. Summary of Dark MIS-CELIV Results.

Materials	Condition	Carrier	Film Thickness [nm]	Voltage Ramp [V s^{-1}]	j_0 [mA cm^{-2}]	t_{2j0} [μs]	t_{tr} [μs]	Mobility [cm^2 $V^{-1}s^{-1}$]
P3HT	Dark	Hole	~120	3.2×10^4	0.5	7.9	10.1	1.3×10^{-4}
		Electron			0.4	12.6	16.1	5.0×10^{-5}
P3HT: PCBM		Hole			0.5	3.7	4.7	5.9×10^{-4}
		Electron			0.4	2.0	2.5	2.1×10^{-3}

importantly, we noticed an interesting phenomenon when comparing Table 1 and Table 2. That is, both hole and electron mobilities of P3HT increased by more than an order of magnitude when laser light was applied whereas in the P3HT:PCBM blend only the value of the hole mobility increased by an order of magnitude and the value of the electron mobility almost remained the same. This verifies the fact that P3HT is much more sensitive to visible light than the UV-absorbing PCBM and hence serves as a light-absorbing layer. Compared to the neat P3HT film, we found that the P3HT:PCBM blend not only had an increased electron mobility and enhanced charge density, but also suppressed the increase of hole mobility in P3HT caused by the light excitation.[53–56] On the other hand, under light illumination the drift of holes and electrons is more balanced in the P3HT:PCBM blend than in P3HT alone, leading to a higher power-conversion efficiency in BHJ photovoltaic cells. This is supported by Table 2, showing that under light illumination, the hole mobility is much larger than the electron mobility in the neat film of P3HT whereas the hole and electron mobilities become almost the same in the blend film of P3HT:PCBM.

2.5. Light MIS-CELIV

To further uncover the dynamics of the charge carriers, we combined the above *j-t* profiles both in the dark and under light with the same voltage offset. For simplicity, **Figure 7** displays the profiles of an electron-only P3HT:PCBM device with a −1 V voltage offset in both dark and light MIS-CELIV measurements with a delay time of 50 μs. When applying different voltage offsets, similar profiles were obtained, regardless of the material used (either P3HT or P3HT:PCBM blend) or the device configuration (either hole-only or electron-only device). It can be seen from Figure 7 that when the same voltage offset of −1 V was applied, the red curve measured under light

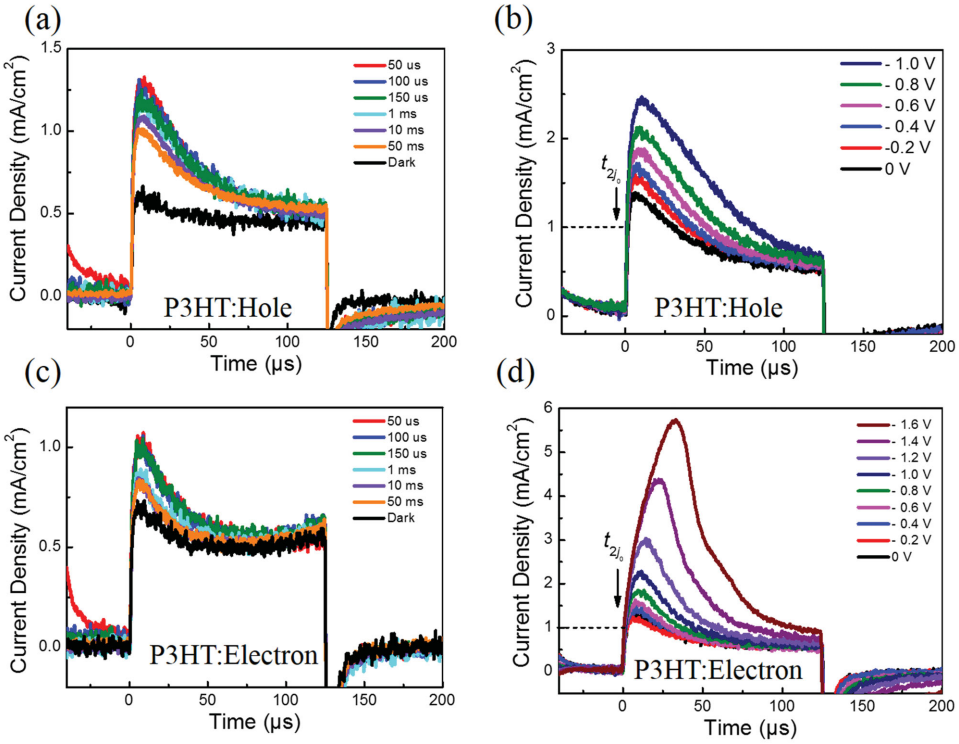

Figure 5. Light MIS-CELIV transients of P3HT. a,b) In hole-only devices: a) transients with various delay times and without voltage offset and b) transients at different voltage offsets with a delay time of 50 μs. c,d) In electron-only devices: c) transients with various delay times and without voltage offset and d) transients at different voltage offsets with a delay time of 50 μs.

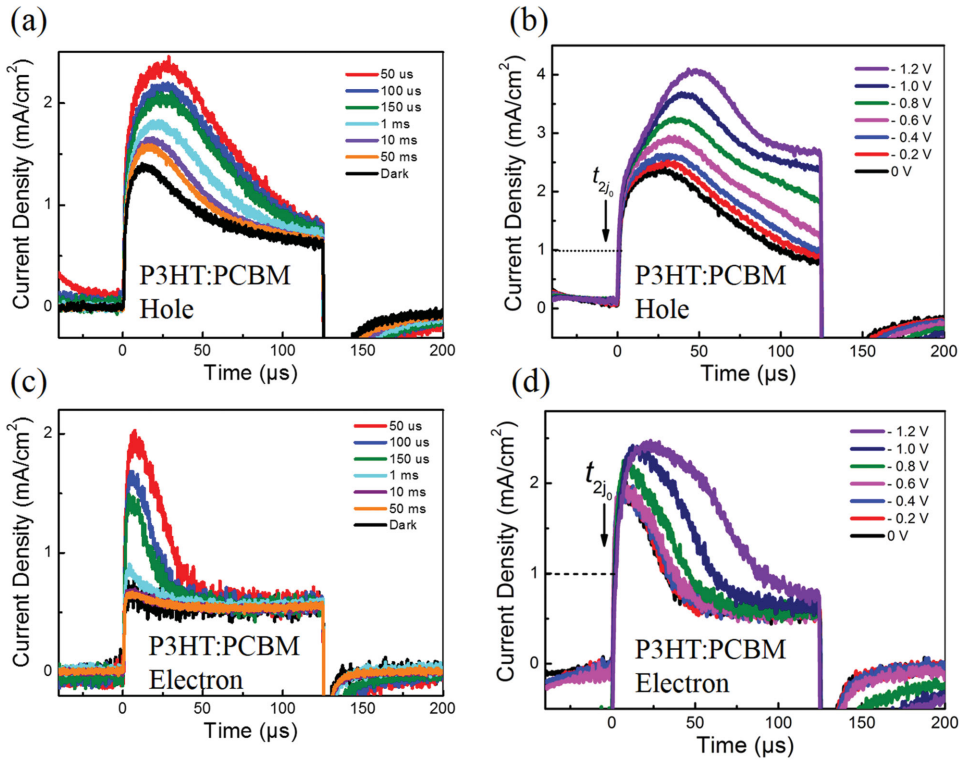

Figure 6. Light MIS-CELIV transients of a P3HT:PCBM blend. a,b) In hole-only devices: a) transients with various delay times and without voltage offset and b) transients at different voltage offsets with a delay time of 50 µs. c,d) In electron-only devices: c) transients with various delay times and without voltage offset and d) transients at different voltage offsets with a delay time of 50 µs.

covered a larger area than that of the blue curve, which was measured in the dark. This is because of the fact that when light was applied, an appreciable amount of photo-generated charge carriers were created, accounting for the extra area, and as a result the amount of total extracted charge carriers thus also increased. Moreover, most of the bias-injected charge carriers (hole or electron) in the dark were localized near the blocking layer, whereas the photo-generated charge carriers (hole and electron) remained in the active layer; as a result, the majority of charge recombination occurred among the photo-generated charge carriers, whereas the recombination between bias-injected and photo-generated charge carriers can be neglected in this work.

In order to clearly be able to distinguish the type of extracted charge carriers, Figure 7 is divided into three areas: a yellow area (i.e., extra area) corresponding to the photo-generated charge carriers, a blue area related to the electrically-injected charge carriers either under light or in the dark, and a white area related to the displacement current, which is the same for the light and dark measurements, and only related to the total capacitance of the device. Thus, this method can be used to compare the photosensitivity of different photovoltaic materials, if they are measured at the same voltage offset regardless of the other conditions of charge-carrier injection. If the yellow area is larger than the blue area at the same voltage offset, for instance, as is the case in this work, it means that more photo-generated charge carriers are created inside and the organic material is more photosensitive. Thus, the light MIS-CELIV is a powerful method of evaluating the efficiency of photoelectric conversion of OPV materials. However, it should be noted that the extraction of photo-generated charge carriers in thin organic films does not necessarily reach the quasi-steady state transport regime where photo-CELIV or any other technique can accurately determine the correct material-dependent mobility value. However, the device-dependent properties can be obtained by this method.

Table 2. Summary of Light MIS-CELIV Results.

Materials	Condition	Carrier	Film Thickness [nm]	Voltage Ramp [V s^{-1}]	j_0 [mA cm^{-2}]	t_{2j0} [µs]	t_{tr} [µs]	Mobility [cm^2 V^{-1} s^{-1}]
P3HT	Light	Hole	~120	3.2×10^4	0.5	1.3	1.7	4.7×10^{-3}
		Electron			0.5	2.2	2.8	1.7×10^{-3}
P3HT: PCBM		Hole			0.5	1.9	2.4	2.3×10^{-3}
		Electron			0.4	1.7	2.1	2.8×10^{-3}

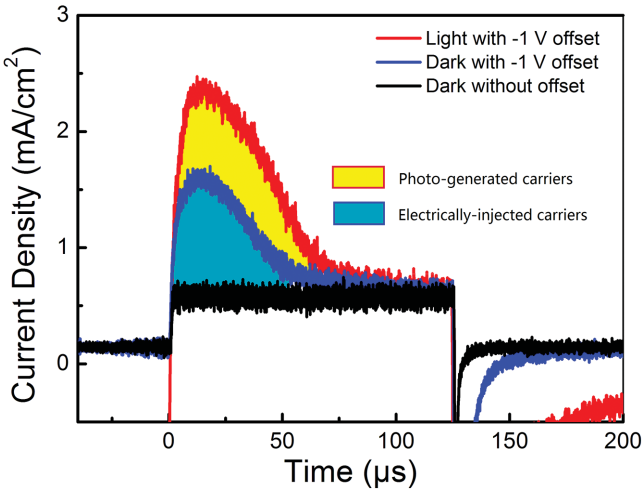

Figure 7. Comparison of light and dark MIS-CELIV transients, exemplified by electron-only P3HT:PCBM devices with a voltage offset of –1 V and a delay time of 50 μs.

3. Conclusions

We have demonstrated that both dark and light MIS-CELIV are effective methods for the characterization of the charge mobility, in which both the hole and electron mobilities can be independently measured in different device configurations. By comparing these dark and light MIS-CELIV results, we were able to reveal the remarkably different influence of light illumination on the charge mobility and recombination process in a neat P3HT film and a P3HT:PCBM blend film. The role of PCBM was suggested not only to increase the electron mobility, but also to suppress the increase of the hole mobility in P3HT caused by light excitation. This further reveals that a balanced hole and electron transport is needed for achieving high efficiencies in benchmark P3HT:PCBM solar cells. Moreover, this newly developed light MIS-CELIV method offers a straightforward means to evaluate the light sensitivity, simply by determining the ratio of the number of photo-generated carriers to that of electrically injected carriers, as these two types of carriers can be clearly distinguished from the extracted *j-t* profiles of the dark and light MIS-CELIV results.

4. Experimental Section

Materials: P3HT and PCBM were obtained from Rieke Metals, Inc. (Item 4002-E, regioregularity 91–94%) and Nano-C, Inc., respectively. Both of them were used as received and stored in the dark in a N_2 atmosphere glovebox. Aluminum pellets (99.9%) and LiF (99.98%) were purchased from R. D. Mathis Co. and Sigma Aldrich, respectively, and used as received. All reagents were purchased from J&K Scientific, Ltd. (China) and used as received.

Device Fabrication: Patterned indium tin oxide (ITO) substrates (12 Ω/□, Thin Film Devices, Inc.) were cleaned sequentially in an ultrasonic bath with deionized water, acetone, and isopropyl alcohol. After drying under nitrogen, the substrates were oxidized in UV-ozone. The substrates were transferred to a N_2-filled glovebox for making the active layer. A solution of P3HT or P3HT:PCBM blend (1:1 by weight) in anhydrous (di)chlorobenzene with a total concentration of 20 mg mL^{-1} was spin-coated onto ITO glass slides at 600 rpm for 60 s, yielding an active layer of around 120 nm thick. The thickness of the active layer was measured on a profilometer. After drying, the active layer was annealed at 120 °C for 20 min. The samples were then loaded into a glovebox-integrated deposition chamber and pumped down to a pressure of $<10^{-4}$ Pa. A sequence of LiF (140 nm) and Al (100 nm) layers were sequentially deposited by thermal evaporation through a shadow mask at a rate of 0.1 Å s^{-1} and 2 Å s^{-1}, respectively. The above procedure was used for the fabrication of hole-only MIS devices. For the fabrication of electron-only MIS devices, a thick LiF (140 nm) layer was first deposited on the ITO at a rate of 0.1 Å s^{-1} and finally a sequence of LiF (1 nm) and Al (100 nm) layers were sequentially deposited at a rate of 0.1 Å s^{-1} and 2 Å s^{-1}, respectively. The active area as defined by the shadow mask was around 0.11 cm^2.

Measurements: For the MIS-CELIV measurements, the device sample was first mounted inside a nitrogen-filled sample holder with a quartz optical window. A linearly increasing voltage pulse in reverse bias (the positive probe was connected to the Al electrode and the negative probe connected to the ITO electrode) was then applied using an arbitrary function generator (Tektronix AFG3021C, 25 MHz bandwidth). The voltage amplitude and ramp were set to 4 V and 3.2×10^4 V s^{-1}, respectively. The current transients were monitored through a 50 Ω load on a Tektronix oscilloscope (DPO4104B, 1 GHz). The RC constants were observed to be significantly smaller than the time scales of interest. Note that the RC constant values of all hole-only and electron-only devices were estimated to be around 1.7×10^{-7} s. This calculation was based on an oscilloscope resistance of 50 Ω and the measured capacitance of the entire diode of ca. 3.4 nF. The t_{tr} was on the order of 10^{-6} s, which was significantly larger than the RC constant, suggesting the calculated mobility values in both Table 1 and 2 are reliable. The transient currents were determined by averaging over 128 frames. To measure the light MIS-CELIV, the sample was excited using a 532-nm Nd:YAG laser (Continuum Minilite II) with a pulse width of 3–5 ns through the ITO side of the device. The laser light intensity was 0.1 mJ cm^{-2}. The delay time was defined. The photo-transients were recorded by varying either the voltage pulse or delay time between laser excitations.

Acknowledgements

This work was supported by National Natural Science Foundation of China (NSFC) under grant No. 51473036 (Z. L.). R. Ö. acknowledges funding from the Academy of Finland project #297055.

Received: October 3, 2015
Revised: November 23, 2015
Published online: January 7, 2016

[1] L. Dou, J. You, Z. Hong, Z. Xu, G. Li, R. A. Street, Y. Yang, *Adv. Mater.* **2014**, *25*, 6642.
[2] W. Cao, J. Xue, *Energy Environ. Sci.* **2014**, *7*, 2123.
[3] C. J. Brabec, V. Dyakonov, E. U. Scherf, *Organic Photovoltaics: Materials, Device Physics, and Manufacturing Technologies*, Wiley-VCH, New York, NJ **2008**.
[4] M. C. Scharber, N. S. Sariciftci, *Prog. Polym. Sci.* **2013**, *38*, 1929.
[5] J. C. Nolasco, G. Ramos-Ortiz, J. L. Maldonado, O. Barbosa-Garcia, B. Ecker, E. v. Hauff, *Appl. Phys. Lett.* **2014**, *104*, 043308.
[6] Z. Liang, A. M. Nardes, J. v. d. Lagemaat, B. A. Gregg, *Adv. Funct. Mater.* **2012**, *22*, 1087.
[7] A. J. Heeger, *Adv. Mater.* **2014**, *26*, 10.
[8] J. Bisquert, G. Garcia-Belmonte, *J. Phys. Chem. Lett.* **2011**, *2*, 1950.
[9] Y. Li, *Acc. Chem. Res.* **2012**, *45*, 723.
[10] C. Groves, *Energy Environ. Sci.* **2013**, *6*, 1546.

[11] L. Wu, H. Zang, Y.-C. Hsiao, X. Zhang, B. Hu, *Appl. Phys. Lett.* **2014**, *104*, 153903.
[12] A. Kumar, G. Lakhwani, E. Elmalem, W. T. S. Huck, A. Rao, N. C. Greenham, R. H. Friend, *Energy Environ. Sci.* **2014**, *7*, 2227.
[13] T. M. Clarke, J. R. Durrant, *Chem. Rev.* **2010**, *110*, 6736.
[14] A. W. Hains, Z. Liang, M. A. Woodhouse, B. A. Gregg, *Chem. Rev.* **2010**, *110*, 6689.
[15] S. R. Cowan, N. Banerji, W. L. Leong, A. J. Heeger, *Adv. Funct. Mater.* **2012**, *22*, 1116.
[16] L. C. C. Elliott, J. I. Basham, K. P. Pernstich, P. R. Shrestha, L. J. Richter, D. M. DeLongchamp, D. J. Gundlach, *Adv. Energy Mater.* **2014**, *4*, 1400356.
[17] A. Foertig, J. Kniepert, M. Gluecker, T. Brenner, V. Dyakonov, D. Neher, C. Deibel, *Adv. Funct. Mater.* **2014**, *24*, 1306.
[18] A. Pivrikas, N. S. Sariciftci, G. Juška, R. Österbacka, *Prog. Photovolt: Res. Appl.* **2007**, *15*, 677.
[19] S. Tiwari, N. C. Greenham, *Opt. Quant. Electron* **2009**, *41*, 69.
[20] A. Kokil, K. Yang, J. Kumar, *J. Polym. Sci. Part B* **2012**, *50*, 1130.
[21] P. N. J. Murgatroyd, *J. Phys. D: Appl. Phys.* **1970**, *3*, 151.
[22] H. Li, L. Duan, D. Zhang, G. Dong, J. Qiao, L. Wang, Y. Qiu, *J. Phys. Chem. C* **2014**, *118*, 6052.
[23] G. Juška, K. Arlauskas, M. Viliunas, K. Genevicius, R. Österbacka, H. Stubb, *Phys. Rev. B* **2000**, *62*, 16235.
[24] B. T. d. Villers, C. J. Tassone, S. H. Tolbert, B. J. Schwartz, *J. Phys. Chem. C* **2009**, *113*, 18978.
[25] K. Genevicius, R. Österbacka, G. Juška, K. Arlauskas, H. Stubb, *Thin Solid Films* **2002**, *403*, 415.
[26] G. Juška, K. Genevicius, K. Arlauskas, R. Österbacka, H. Stubb, *Phys. Rev. B* **2002**, *65*, 233208.
[27] A. J. Morfa, A. M. Nardes, S. E. Shaheen, N. Kopidakis, J. v. d. Lagemaat, *Adv. Funct. Mater.* **2011**, *21*, 2580.
[28] F. Laquai, G. Wegner, H. Bässler, *Phil. Trans. R. Soc. A* **2007**, *365*, 1473.
[29] H. Scher, E. W. Montroll, *Phys. Rev. B* **1975**, *12*, 2455.
[30] Z. Bao, A. Dodabalapur, A. J. Lovinger, *Appl. Phys. Lett.* **1996**, *69*, 4108.
[31] Q. Wei, K. Hashimoto, K. Tajima, *ACS Appl. Mater. Interfaces* **2011**, *3*, 139.
[32] A. J. Mozer, N. S. Sariciftci, A. Pivrikas, R. Österbacka, G. Juška, L. Brassat, H. Bässler, *Phys. Rev. B* **2005**, *71*, 035214.
[33] M. J. Tan, W. P. Goh, J. Li, G. Pundir, V. Chellappan, Z. K. Chen, *ACS Appl. Mater. Interfaces* **2010**, *2*, 1414.
[34] L. M. Andersson, A. Melianas, Y. Infahasaeng, Z. Tang, A. Yartsev, O. Inganäs, V. Sundström, *J. Phys. Chem. Lett.* **2013**, *4*, 2069.
[35] A. Armin, M. Velusamy, P. L. Burn, P. Meredith, A. Pivrikas, *Appl. Phys. Lett.* **2012**, *101*, 083306.
[36] G. Sliauzys, G. Juška, K. Arlauskas, A. Pivrikas, R. Österbacka, M. Scharber, A. Mozer, N. S. Sariciftci, *Thin Solid Films* **2006**, *511–512*, 224.
[37] S. Khademi, J. Y. Song, P. B. Wyatt, T. Kreouzis, W. P. Gillin, *Adv. Mater.* **2012**, *24*, 2278.
[38] N. Camaioni, F. Tinti, A. D. Esposti, S. Righi, O. Usluer, S. Boudiba, D. A. M. Egbe, *Appl. Phys. Lett.* **2012**, *101*, 053302.
[39] A. Armin, G. Juška, M. Ullah, M. Velusamy, P. L. Burn, P. Meredith, A. Pivrikas, *Adv. Energy Mater.* **2014**, *4*, 1300954.
[40] C. Li, L. Duan, Y. Sun, H. Li, Y. Qiu, *J. Phys. Chem. C* **2012**, *116*, 19748.
[41] S. Sandén, O. J. Sanberg, Q. Xu, J.-H. Smått, G. Juška, M. Lindén, R. Österbacka, *Phys. Chem. Chem. Phys.* **2012**, *14*, 14186.
[42] S. Sandén, O. J. Sanberg, Q. Xu, J.-H. Smått, G. Juška, M. Lindén, R. Österbacka, *Org. Electron.* **2014**, *15*, 3506.
[43] S. T. Zhang, X. M. Ding, J. M. Zhao, H. Z. Shi, J. He, Z. H. Xiong, H. J. Di, E. G. Obbard, Y. Q. Zhan, W. Huang, X. Y. Hou, *Appl. Phys. Lett.* **2004**, *84*, 425.
[44] A. J. Mozer, G. Dennler, N. S. Sariciftci, M. Westerling, A. Pivrikas, R. Österbacka, G. Juška, *Phys. Rev. B* **2005**, *72*, 035217.
[45] S. Chen, K. R. Choudhury, J. Subbiah, C. M. Amb, J. R. Reynolds, F. So, *Adv. Energy Mater.* **2011**, *1*, 963.
[46] S. A. Choulis, Y. Kim, J. Nelson, D. D. C. Bradley, M. Giles, M. Shkunov, I. McCulloch, *Appl. Phys. Lett.* **2004**, *85*, 3890.
[47] R. Mauer, M. Kastler, F. Laquai, *Adv. Funct. Mater.* **2010**, *20*, 2085.
[48] H.-G. Flesch, R. Resel, C. R. McNeill, *Org. Electron.* **2009**, *10*, 1549.
[49] B. Huang, E. Glynos, B. Frieberg, H. Yang, P. F. Green, *ACS Appl. Mater. Interfaces* **2012**, *4*, 5204.
[50] H. Yang, E. Glynos, B. Huang, P. F. Green, *J. Phys. Chem. C* **2013**, *117*, 9590.
[51] X. Shen, V. V. Duzhko, T. P. Russell, *Adv. Energy Mater.* **2013**, *3*, 263.
[52] A. M. Ballantyne, L. Chen, J. Dane, T. Hammant, F. M. Braun, M. Heeney, W. Duffy, I. McCulloch, D. D. C. Bradley, J. Nelson, *Adv. Funct. Mater.* **2008**, *18*, 2373.
[53] M. P. d. Haas, J. M. Warman, T. D. Anthopoulos, D. M. d. Leeuw, *Adv. Funct. Mater.* **2006**, *16*, 2274.
[54] V. D Mihailetch, J. K. J. v. Duren, P. W. M. Blom, J. C. Hummelen, R. A. J. Janssen, J. M. Kroon, M. T. Rispens, W. J. H. Verhees, M. M. W. Martijn, *Adv. Funct. Mater.* **2003**, *13*, 43.
[55] J. Schafferhans, C. Deibel, V. Dyakonov, *Adv. Energy Mater.* **2011**, *1*, 655.
[56] G. Ren, C. W. Schlenker, E. Ahmed, S. Subramaniyan, S. Olthof, A. Kahn, S. Ginger, S. A. Jenekhe, *Adv. Funct. Mater.* **2013**, *23*, 1238.